Mapping transport properties of halide perovskites via short time dynamics scaling laws and sub-nanosecond time resolution imaging

Guillaume Vidon,[1,2,*] Stefania Cacovich,[1,2] Marie Legrand,[1,3] Armelle Yaiche,[1,3] Daniel Ory,[1,3] Daniel Suchet,[1,2] Jean-Baptiste Puel,[1,3] and Jean-François Guillemoles[1,2,†]

[1] *IPVF, Institut Photovoltaïque d'Ile-de-France, 18 Boulevard Thomas Gobert, 91120 PALAISEAU, France*
[2] *Institut Photovoltaïque d'Ile de France, UMR IPVF 9006, CNRS, Ecole Polytechnique, Institut Polytechnique de Paris, PSL Chimie ParisTech, IPVF SAS, 91120 PALAISEAU, France*
[3] *EDF RD, 18 Boulevard Thomas Gobert, 91120 PALAISEAU, France*

(Dated: October 27, 2021)

Supplemental Material

CONTENTS

* guillaume.vidon@ipvf.fr
† jean-francois.guillemoles@cnrs.fr

I. MODEL ADDITIONAL DETAILS

A. Interpretation of the defect related densities

In the main article, the bulk and interface defect related densities N_{bulk}, N_{top} and N_{bot} are introduced. We give here some elements of interpretation of these densities. They are to be considered when the defects are close to one of the bands. By considering the conduction band, we can write $N_{bulk} = \frac{N_c}{2}\exp\left(\frac{E_t - E_c}{kT}\right)$ with the effective density of state for the conduction band N_c, the energy of the defect E_t, the energy of the conduction band E_c, k Boltzmann constant and T the carrier temperature. For many absorbers, such as Silicon or III-V materials, defects lying energetically deep in the band gap are the major channel of recombination [31].For such defects, the density N_{bulk} is negligible compared to Δn. However, if the defects are close to one of the band edges, as could be the case for lead halide perovskites [3],N_{bulk} may not be neglected in front of $\Delta n(z,t)$ depending on position and time. Specifically, at long time after the pulse, when the photogenerated carrier density has plummeted, N_{bulk} should be considered. Conversely, N_{bulk} can be neglected at short time where the photogenerated carrier density is still high.

B. Computation of the scaling

We need to compute in our model framework the following quantity:

$$\left.\frac{dI_{PL}^{norm}}{dt}\right|_{t=0} = \frac{1}{I_{PL}(t=0)} \times \left.\frac{dI_{PL}}{dt}\right|_{t=0} \tag{1}$$

We can first compute $I_{PL}(t=0)$ which given the definition yields:

$$I_{PL}(t=0) = A \times \int_0^L \Delta n^2(z', t=0)\, dz' = A n_\gamma^2 \alpha^2 \int_0^L e^{-2\alpha z'}\, dz' = \frac{A n_\gamma^2 \alpha}{2}\left(1 - e^{-2\alpha L}\right) \tag{2}$$

For the derivative we have:

$$\left.\frac{dI_{PL}}{dt}\right|_{t=0} = 2A \times \int_0^L \Delta n(z', t=0) \frac{d\Delta n}{dt}(z', t=0) dz' \tag{3}$$

From the drift-diffusion equation given in the main, along with the definitions of the PL signal and the recombination terms one may compute:

$$\begin{aligned}\frac{dI_{PL}}{dt} = -2A\left[k_1 \int_0^L \frac{\Delta n^3}{\Delta n + N_{bulk}}\, dz' + k_2 \int_0^L \Delta n^3\, dz' + S_{top}\frac{\Delta n^3(z=0,t)}{\Delta n(z=0,t) + N_{top}} + S_{bot}\frac{\Delta n^3(z=L,t)}{\Delta n(z=L,t) + N_{bot}}\right] \\ -2AD\int_0^L \left(\frac{\partial \Delta n}{\partial z}\right)^2 dz'\end{aligned} \tag{4}$$

A similar equation may also be found in [21].We then make the main approximation that we can compute the integrals with a carrier distribution equal to the Beer-Lambert initial condition. We need compute the following integrals valid within this approximation:

$$\int_0^L \Delta n^3\, dz' = \frac{n_\gamma^3 \alpha^2}{3}\left(1 - e^{-3\alpha L}\right) \tag{5}$$

$$\int_0^L \left(\frac{\partial \Delta n}{\partial z}\right)^2 dz' = \left(-n_\gamma \alpha^2\right)^2 \int_0^L e^{-2\alpha z'}, dz' = \frac{n_\gamma^2 \alpha^3}{2}\left(1 - e^{-2\alpha L}\right) \tag{6}$$

The first integral in Equation 4 is computed in the following section, general result being :

$$I = \int_0^L dz \frac{\Delta n^3}{\Delta n + N_{bulk}} = n_\gamma^2 \alpha \left[\left(\frac{N_{bulk}}{n_\gamma \alpha}\right)^2 \ln\left(\frac{\frac{N_{bulk}}{n_\gamma \alpha} + 1}{\frac{N_{bulk}}{n_\gamma \alpha} + e^{-\alpha L}}\right) + \frac{1}{2} - \frac{N_{bulk}}{n_\gamma \alpha} - \frac{1}{2}e^{-\alpha L}\left(e^{-\alpha L} - 2\frac{N_{bulk}}{n_\gamma \alpha}\right)\right] \tag{7}$$

The top and bottom recombination terms give:

$$S_{top}\frac{\Delta n^3(z=0,t)}{\Delta n(z=0,t)+N_{top}} = n_\gamma^2\alpha^2 S_{top}\frac{1}{1+\frac{N_{top}}{n_\gamma\alpha}} \tag{8}$$

$$S_{bot}\frac{\Delta n^3(z=L,t)}{\Delta n(z=L,t)+N_{bot}} = n_\gamma^2\alpha^2 S_{bot}e^{-2\alpha L}\frac{1}{1+\frac{N_{bot}e^{-\alpha L}}{n_\gamma\alpha}} \tag{9}$$

Finally one can compute the scaling in the general case. However this general form can be simplified by considering the case where $e^{-\alpha L} \approx 0.039 \ll 1$ (leading to simplify Eq. 2, Eq. 5, Eq.6, and neglect Eq.9 in front of Eq.8) and $\frac{N_{bulk}}{n_\gamma\alpha} \ll 1$ (leading to simplify I), and $\frac{N_top}{n_\gamma\alpha} \ll 1$ (leading to simplify Eq.8). The case of the approximation of the integral I, appearing as a factor of the term proportional to k_1 in Eq 4, is discussed below. This gives us a simplified scaling valid in the high absorption and deep defects approximation :

$$\left.\frac{dI_{PL}^{norm}}{dt}\right|_{t=0} = -2\left[k_1 + 2\alpha S_{top} + \alpha^2 D\right] - \frac{4}{3}k_2\alpha n_\gamma \tag{10}$$

C. Computation of the integral I

We need to compute the integral given by:

$$I = \int_0^L dz\frac{\Delta n^3}{\Delta n + N_{bulk}} \tag{11}$$

when the density is equal at short time to $\Delta n(z, t=0) = n_\gamma\alpha e^{-\alpha z}$. This yields us:

$$I = (n_\gamma\alpha)^2\int_0^L dz\frac{e^{-3\alpha z}}{e^{-\alpha z}+\frac{N_{bulk}}{n_\gamma\alpha}} \tag{12}$$

A change of variables $x = \exp(-\alpha z)$ with $dx = -\alpha x dz$ yields:

$$I = n_\gamma^2\alpha\int_{e^{-\alpha L}}^1 dx\frac{x^2}{x+\frac{N_{bulk}}{n_\gamma\alpha}} \tag{13}$$

A primitive of $\frac{x^2}{x+a}$ is $a^2\ln(a+x)+\frac{1}{2}x(x-2a)$. This formula gives us the result:

$$I = n_\gamma^2\alpha\left[\left(\frac{N_{bulk}}{n_\gamma\alpha}\right)^2\ln\left(\frac{\frac{N_{bulk}}{n_\gamma\alpha}+1}{\frac{N_{bulk}}{n_\gamma\alpha}+e^{-\alpha L}}\right)+\frac{1}{2}-\frac{N_{bulk}}{n_\gamma\alpha}-\frac{1}{2}e^{-\alpha L}\left(e^{-\alpha L}-2\frac{N_{bulk}}{n_\gamma\alpha}\right)\right] \tag{14}$$

This formula can be recast in the following way:

$$I = \frac{n_\gamma^2\alpha}{2}\times C\left(\frac{N_{bulk}}{n_\gamma\alpha}, e^{-\alpha L}\right) \tag{15}$$

With C a function described by:

$$C\left(\frac{N_{bulk}}{n_\gamma\alpha}, e^{-\alpha L}\right) = 2\left[\left(\frac{N_{bulk}}{n_\gamma\alpha}\right)^2\ln\left(\frac{\frac{N_{bulk}}{n_\gamma\alpha}+1}{\frac{N_{bulk}}{n_\gamma\alpha}+e^{-\alpha L}}\right)+\frac{1}{2}-\frac{N_{bulk}}{n_\gamma\alpha}-\frac{1}{2}e^{-\alpha L}\left(e^{-\alpha L}-2\frac{N_{bulk}}{n_\gamma\alpha}\right)\right] \tag{16}$$

We will show that in a wide range of parameters one can make the approximation that $C\left(\frac{N_{bulk}}{n_\gamma\alpha}, e^{-\alpha L}\right) \approx 1$. In our study, $e^{-\alpha L} \approx e^{-3.25} \approx 0.039$, and in Figure 1 we plot C as a function of $\frac{N_{bulk}}{n_\gamma\alpha}$ and $e^{-\alpha L}$ and report the expected range of our study by a red polygon. To draw this polygon, we allow α to vary $\pm 10\%$ around the value $\alpha = 6.5\times10^4$ cm^{-1}. We see that the value of C depends weekly on both variable (a change of approximately 20% of C for a change of almost 2 orders of magnitude of $\frac{N_{bulk}}{n_\gamma\alpha}$). As long as both $e^{-\alpha L} \ll 1$ and $\frac{N_{bulk}}{n_\gamma\alpha} \ll 1$, the value of C can be considered constant to a first approximation: $C = 1 \pm 0.25$.

Therefore, for our parameter set, we can approximate that:

$$I = \frac{n_\gamma^2\alpha}{2} \tag{17}$$

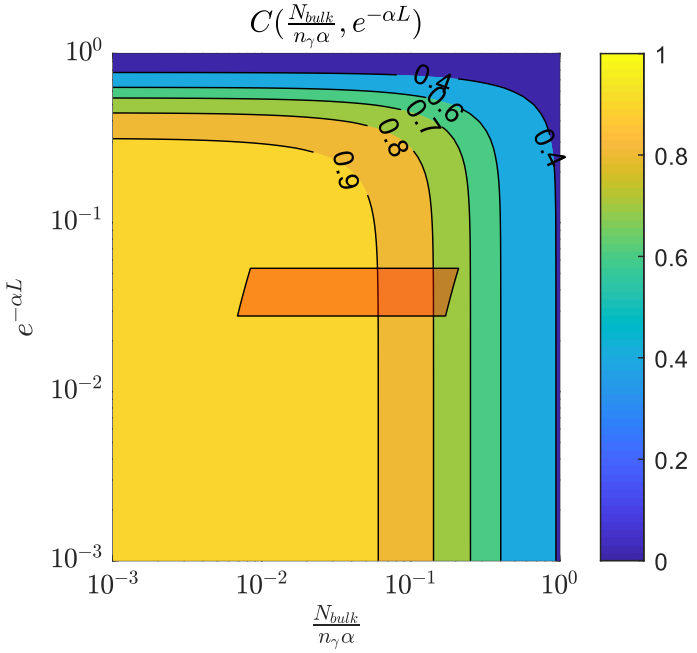

FIG. 1. Plotting the map of C as a function of $e^{-\alpha L}$ and $\frac{N_{bulk}}{n_\gamma \alpha}$. The red rectangle corresponds to our case of interest, with $L = 500nm$ and $\alpha = 6.5 \times 10^4\ cm^{-1}$ varied from $\pm 10\%$, and $n_\gamma \in [4, 100] \times 10^{11}$ ph.cm^{-2} and $N_{bulk} = 4.9 \times 10^{15}\ cm^{-3}$ (as found by our fitting method, see the corresponding section below). In that region, the value of C is close to 1 at 25%.

D. Taking Auger Recombination into account

In the main text, Auger recombination are not considered. However, the model can be generalized to include them. We consider the added term $k_3(\Delta n)^3$ in the recombination term, with k_3 the Auger coefficient, so that the recombination term becomes:

$$R = k_1 \frac{(\Delta n)^2}{\Delta n + N_{bulk}} + k_2(\Delta n)^2 + k_3(\Delta n)^3 \tag{18}$$

To further simplify, we take the approximation that $\frac{N_{bulk}}{n_\gamma \alpha} \ll 1$. The scaling law can be computed with the added Auger term, following the same demonstration as exposed above. One finds:

$$\left.\frac{dI_{PL}^{norm}}{dt}\right|_{t=0} = -2\left[k_1 + 2\alpha S_{top} + \alpha^2 D\right] - \frac{4}{3}k_2 \alpha n_\gamma - k_3 \alpha^2 n_\gamma^2 \tag{19}$$

When taking Auger recombination into account, one finds an order 2 polynomial in the laser fluence n_γ. Experimentally, we did not observe this behavior, which justifies the fact that we neglected Auger recombination.

E. The role of photon recycling

1. *Description of the model*

In this subsection, we discuss the role of photon recycling on the exhibited scaling. To do so, we implement the model of Ansari-Rad and Bisquert [38].This model couples the density of photons, noted Γ, and the density of carriers, Δn, via two drift diffusion equations. A coupling parameter β between them is introduced in [38]. The couple of equations in the present case can be written as:

$$\frac{\partial \Delta n}{\partial t}(z,t) = D\frac{\partial^2 \Delta n}{\partial z^2}(z,t) - k_1 \frac{(\Delta n)^2}{\Delta n + N_{bulk}} - k_2(\Delta n)^2 + \beta\Gamma \tag{20}$$

$$\frac{\partial \Gamma}{\partial t}(z,t) = D_\Gamma \frac{\partial^2 \Gamma}{\partial z^2}(z,t) + k_2(\Delta n)^2 - \beta\Gamma \tag{21}$$

with D_Γ the effective diffusion coefficient for photons, β the coupling parameter. These equations are accompanied with boundary conditions. For the equation of carriers on Δn, they are given in the main paper. For the photon density Γ they are as follows:

$$D_\Gamma \frac{\partial \Gamma}{\partial z}(z=0,t) = S_{top-\Gamma}\Gamma(z=0,t) \tag{22}$$

$$D_\Gamma \frac{\partial \Gamma}{\partial z}(z=L,t) = -S_{bot-\Gamma}\Gamma(z=L,t) \tag{23}$$

The initial condition for Γ is set at $\Gamma(z, t=0) = 0$.

In this framework, one can define the output PL to be proportional to $\Gamma(z=0,t)$, i.e. to the output flow of photons via the top surface.

We used this framework to estimate the impact of photon recycling. To do so, we simulated the decays using these formulae and measured numerically the scaling law on the obtained decays. Our main parameter is the re-absorption coefficient α_{reabs}. In [38],formulae are given to link the effective diffusion coefficient for photons D_Γ, the coupling parameter β and the outcoupling parameters $S_{top-\Gamma}$ and $S_{bot-\Gamma}$ to the re-absorption coefficient α_{reabs}, the speed of light in vacuum c and n_r the refractive index of the perovskite layer.

$$D_\Gamma = \frac{c}{n_r \alpha_{reabs}} \tag{24}$$

$$\beta = \frac{\alpha_{reabs} c}{n_r} \tag{25}$$

$$S_{top-\Gamma} = S_{bot-\Gamma} = \frac{c}{2n_r} \tag{26}$$

2. Parameters of the model

For the recombination and charge carrier parameters, we used the parameters given in Table SI. For the photon parameters, we used a value of $n_r = 2.5$ and varied α_{reabs} in the range 10^2 to 10^4 cm^{-1}.

3. Results of the model

The results are presented in Figure 2. In (a) two decays obtained at the highest fluence (10^{13} ph.cm^{-2}) are presented for the case without photon recycling and the case with photon recycling with a reabsorption coefficient of $\alpha_{reabs} = 10^2 cm^{-1}$. We observe no notable difference. In (b) we plot the scaling law obtained for three distinct scenarii: (i) with no photon recycling, (ii) with photon recycling $\alpha_{reabs} = 10^2 cm^{-1}$, (iii) with photon recycling $\alpha_{reabs} = 10^4 cm^{-1}$. All scalings show very similar slopes and intercept. We found an impact of the photon recycling only for $\alpha_{reabs} = 2 \times 10^4 cm^{-1}$ which is a very high value for the absorption coefficient around the emission peak. Therefore, we observe no impact of photon recycling on the scaling for sensible values of reabsorption coefficient. We conclude that in our case, the internal value of the radiative recombination coefficient is close to the external one.

4. Impact of photon-outcoupling at the surfaces

The impact of the photon outcoupling parameter at the surface is studied here. We start from using the value suggested by Ansari-Rad and Bisquert and modify it with a increase and reduction of one order of magnitude. Two cases are considered: one with low reabsorption ($\alpha_{reabs} = 10^2$ cm^{-1}) and one with high reabosrption ($\alpha_{reabs} = 10^4$ cm^{-1}). Result are shown in Figure 3 (a) and (b). In the low reabsorption coefficient case, no impact is observed of the outcoupling parameter on the scaling. In the high reabsorption case, an impact is shown on the scaling. We have two observations. One, the impact on the slope is limited to $\pm 20\%$ even though we changed the outcoupling parameter by one order of magnitude. This would be below our measurement sensibility. Two, all scalings show a similar intercept. This means that the outcoupling parameter does not affect the intercept of the scaling. We conclude that in the present case, the outcoupling parameter has but low impact on the observed external radiative recombination coefficient. In a more general case, the observed slope of the scaling would be modified by light outcoupling parameters: the value of k_2 extracted in this case is what we define as the external radiative recombination coefficient.

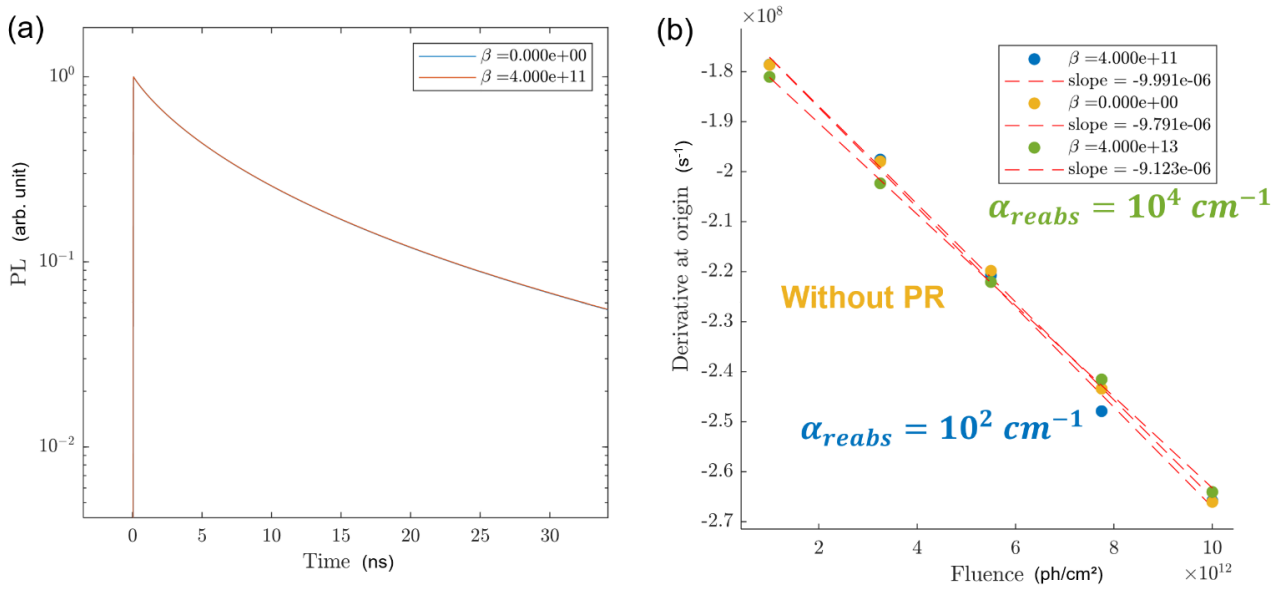

FIG. 2. Impact of photon recycling. (a) TR-PL decay at high fluence (1e13 ph/cm^2) simulated with (blue) and without (orange) photon recycling taken into account. The reabsorption coefficient was set to $10^2\ cm^{-1}$. (b) Scaling law at short time as a function of fluence for the case with (blue and green) and without (yellow) photon recycling.

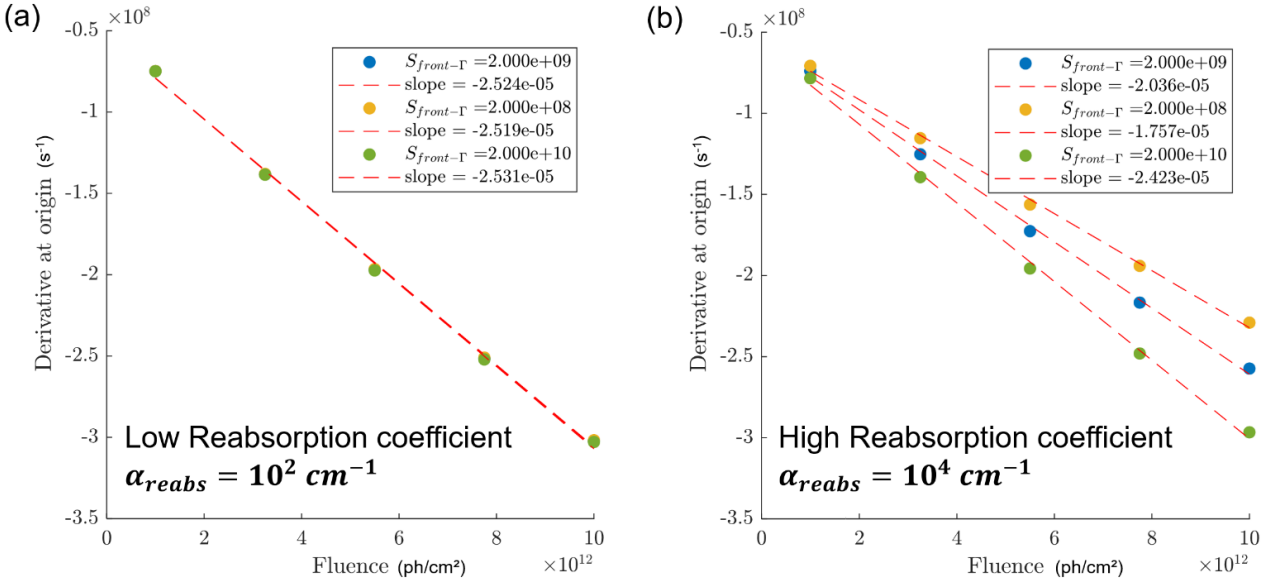

FIG. 3. Impact of the outcoupling surface parameter on the derived scaling law. (a) Case of low reabsorption ($\alpha_{reabs} = 10^2$ cm^{-1}) – we see no impact of the surface outcoupling parameter (all the curves are superimposed). (b) Case of high reabsorption ($\alpha_{reabs} = 10^4$ cm^{-1}), for three different outcoupling parameters: reference value from Ansari-Rad and Bisquert, one order of magnitude less, one order of magnitude more. The impact on slope of the scaling remains in the ± 20% range.

F. Low absorption regime

We report here the generalized case of the Scaling Law (Eq. 7 in the Main, and Eq. S10) for laser wavelengths where the approximation $e^{-\alpha(\lambda)L} \ll 1$ cannot be made. We place ourselves in the case where the defect related densities can be neglected meaning, specifically in the case where N_{bulk},N_{top},$N_{bot} \ll n_\gamma \alpha e^{-\alpha L}$. In this case, the generalized scaling we obtain is the following:

$$\left.\frac{dI_{PL}^{norm}}{dt}\right|_{t=0} = -2k_1 - 2\alpha^2 D - \frac{4\alpha}{1-e^{-2\alpha L}}\left(S_{top} + S_{bot}e^{-2\alpha L}\right) - \frac{4}{3}k_2\alpha\left(\frac{1-e^{-3\alpha L}}{1-e^{-2\alpha L}}\right)n_\gamma \tag{27}$$

In this case, the bottom surface recombination appears, even if it is scaled by a factor $e^{-2\alpha L}$ compared to the top surface recombination coefficient. In the high absorption case considered in our study, we have $e^{-\alpha L} \approx e^{-3.25} \approx 0.039$. This gives the following numerical results for the coefficients:

$$\left.\frac{dI_{PL}^{norm}}{dt}\right|_{t=0} = -2k_1 - 2\alpha^2 D - 4\alpha\underbrace{\frac{1}{1-e^{-2\alpha L}}}_{\approx 1.0015}\left(S_{top} + S_{bot}\underbrace{e^{-2\alpha L}}_{\approx 0.0015}\right) - \frac{4}{3}k_2\alpha\underbrace{\left(\frac{1-e^{-3\alpha L}}{1-e^{-2\alpha L}}\right)}_{\approx 1.0014}n_\gamma \tag{28}$$

This computation justifies our assumption of high aborption that gives the equation given in the main text, see Eq. 7 and Eq. S10. However, in the case of a laser light closer to the gap of the material under study, the condition $e^{-\alpha L} \ll 1$ may be false and the correct formula for the scaling is given by Eq. S27.

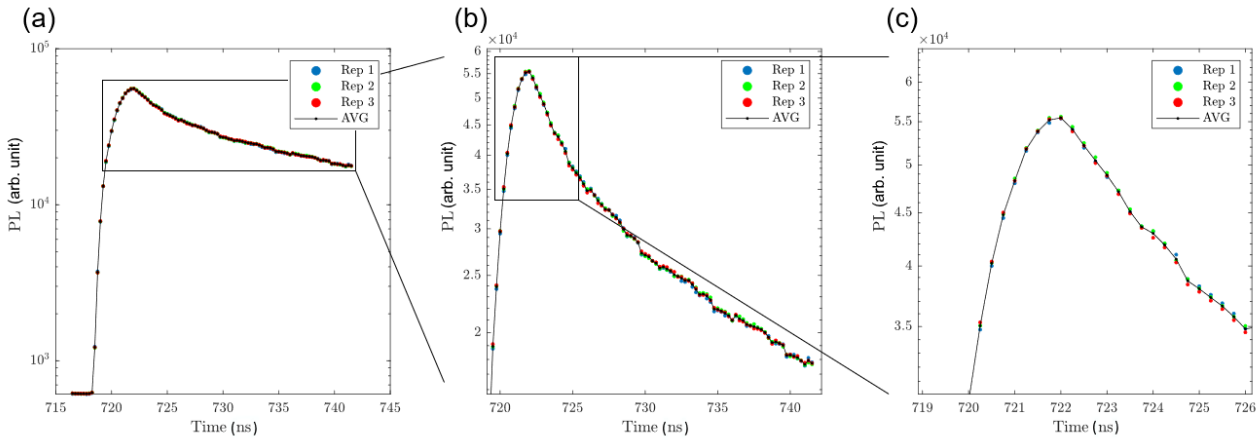

FIG. 4. Example of repetitions (labelled 'Rep') of acquisitions (a) General view (b) Zoom 1 (c) Zoom 2. Three acquisitons are performed in a row with a 5s waiting time. We saw a very good stability of the material under measurement. No light soaking effects were noticed. The average of Rep 2 / Rep 1 is 1.0026 ± 0.0077, and for Rep 3 / Rep 1 it is 1.0012 ± 0.0085. The fluence was $8.52 \times 10^{11} ph.cm^{-2}$.

II. UNCERTAINTIES ON THE EXPERIMENTAL DATA

A. Repetition of the experiments

Each acquisition was repeated 3 times to verify reproducibility and stability of the material. Very good stability was observed as examplified by Figure 4.

B. Numerical determination of the derivative at short time

To measure the numerical value of the derivative at short time we fit linearly the function $\log(I_{PL}(t)/I_{PL}(t=0))$ between 0.5 and 2.5ns. This linear fitting allows to extract a slope as well as its uncertainty that corresponds to the initial derivative. The Matlab functions `fit` and `confint` are used.

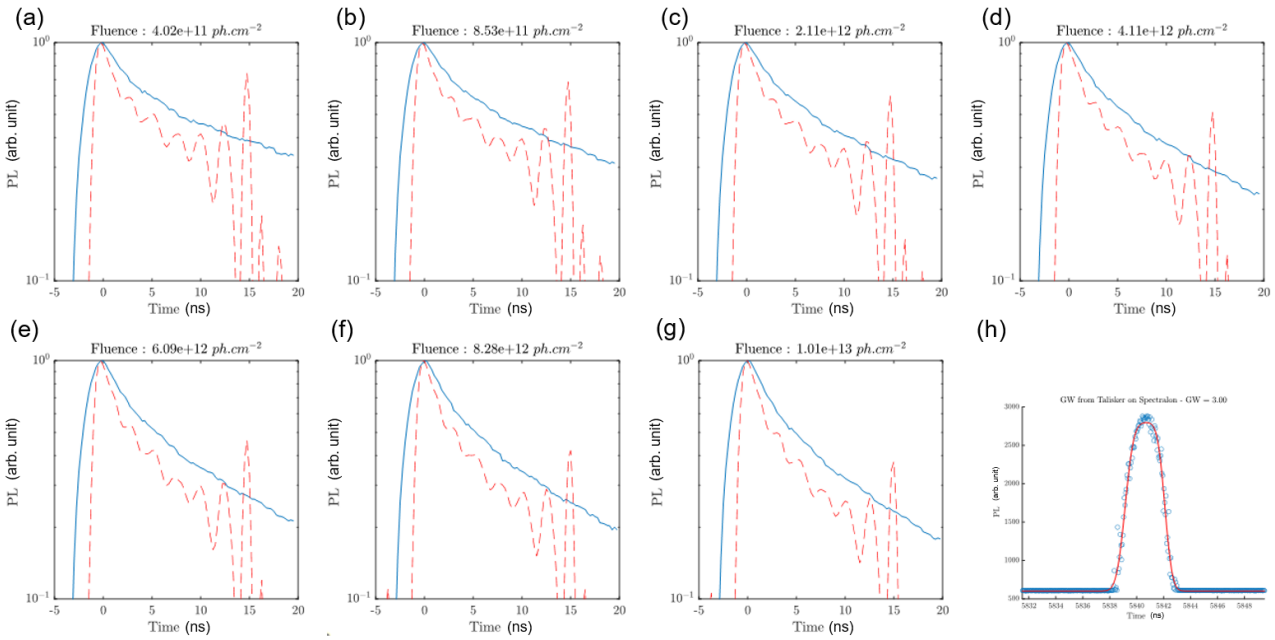

FIG. 5. (a-g) Deconvolution of the seven highly-resolved decays with Wiener filter. (Blue solid line) Original decays (red dotted line) Deconvoluted decays. For this deconvolution the parameter $K = 0.1$. All curves are normalized to their maximal value. We can observe oscillations after 3ns approximately after the maximum value is reached. (h) Temporal shape of the 3ns-long gate of the camera. (Blue points) Experimental data ; (Red line) Phenomenological fit.

III. TEMPORAL DECONVOLUTION OF THE SIGNAL

A. Wiener Filter

A deconvolution algorithm via Fourier transform is used. We measured the temporal shape of the gate we used by imaging the laser pulse (duration ¡70ps) on a Spectralon diffuser. The temporal shape of the gate was acquired and fitted with a model using complementary error-functions, see Figure 5 (h). The model for the gate temporal shape is:

$$h(t) = \frac{1}{2}\left[\mathrm{erfc}\left(\frac{t-t_1}{\Delta t_1}\right) - \mathrm{erfc}\left(\frac{t-t_2}{\Delta t_2}\right)\right] \tag{29}$$

The fitted parameters for our gate are : $t_1 = -(1.361 \pm 0.017)ns$, $\Delta t_1 = (0.719 \pm 0.033)ns$, $t_2 = (1.592 \pm 0.016)ns$, $\Delta t_2 = (0.619 \pm 0.030)ns$. A noise constant of 600 counts was added.

To deconvolve the signal, a Wiener fielter is used. If $S = F(s)$ and $H = F(h)$ are the Fourier transform of the signal and of our temporal gate, then we apply the following to obtain our deconvolved signal s_d:

$$s_d = F^{-1}\left(\frac{S}{H}\frac{|H|^2}{|H|^2 + K}\right) \tag{30}$$

with K a chosen coefficient. The computation are performed using Fast Fourier Transform algorithms, and the resulting decay with $K = 0.1$ are shown in Figure 5 (a-g). The deconvolution works well only for the short time and high signal-to-noise-ratio temporal region, which is the one of interest for us.

The scaling law may be computed for the convoluted and for the deconvoluted cases. Figure 6 shows the two cases. We observe that temporal convolution has an impact on both the intercept and the slope. The convoluted slope is approximately 50% of the deconvoluted one, which is compatible with our simulations of the impact of deconvolution. The intercept is slightly improved by the deconvolution algorithm.

The influence of the parameter K on the obtained decays and scaling laws is shown in Figure 7. In (a) and (b) the impact on the the deconvoluted decays is shown. Higher noise is observed when lowering K towards the end of the decay, but sharper results are obtained at the beginning, (a). One can see that the oscillations in the less intense part of the signal become comparable to the maximal value observed. In (b), we see that increasing K gives a smoother result but closer to the original convoluted one. The impact of K on the scaling is shown in (c). The slope is mainly

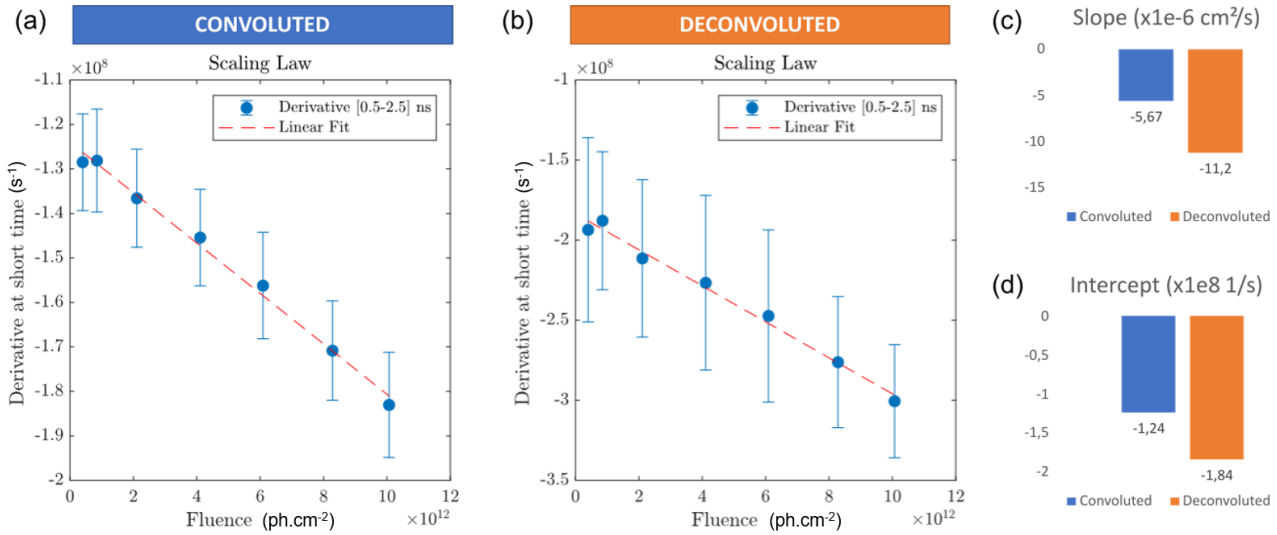

FIG. 6. (a) Scaling computed on original decays. (b) Scaling computed on deconvoluted decays. The parameter $K = 0.1$. (c) Comparison of the obtain fitted slope (d) Comparison of the obtained fitted intercept.

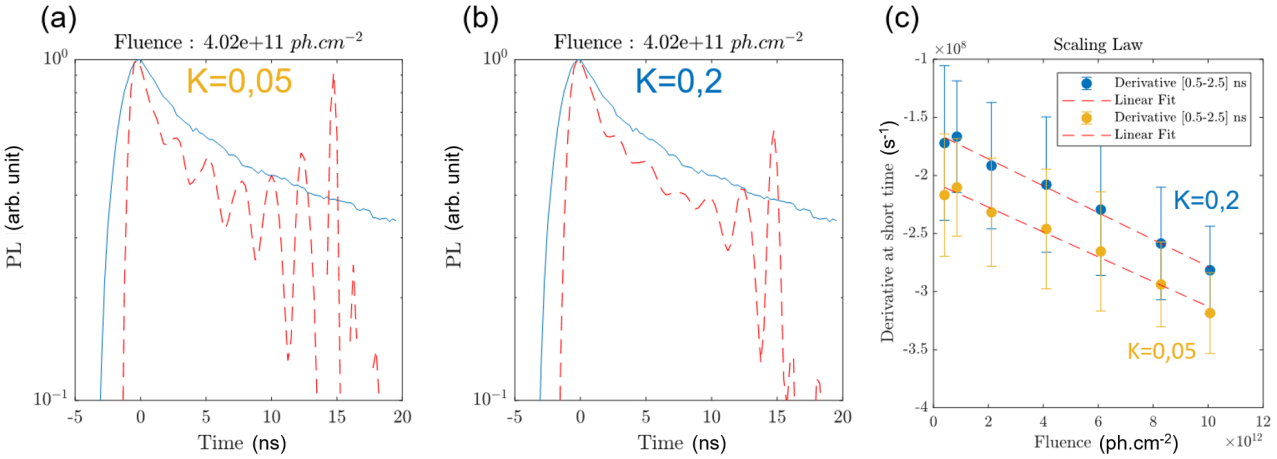

FIG. 7. Influence of the parameter K. (a-b) Similar decay deconvoluted with (a) $K = 0.05$ and $K = 0.2$. (c). Comparisons of the scaling laws computed on deconvoluted decays with $K = 0.05$ (yellow) and $K = 0.2$ (blue). A linear fit is performed for both. For the blue points with $K = 0.2$, Slope : $-1.16e-05 \pm 1.28e-06$ $cm^2 s^{-1}$ Intercept: $-1.63e+08 \pm 7.32e+06$ s^{-1}. For the yellow points with $K = 0.05$, Slope : $-1.07e-05 \pm 1.52e-06$ $cm^2 s^{-1}$ Intercept: $-2.06e+08 \pm 8.71e+06$ s^{-1}.

not affected by K with a 10% change when K varies from 0.05 to 0.2. The intercept is more sensible to a change of K with a 25% change in the intercept when K is divided by 4. The results still are compatible when considering the error-bars. We conclude that K does not affect the slope, hence does not affect the extracted value of αk_2 . We chose $K = 0.1$ as an intermediate solution, with K small enough to have an effect of deconvolution but K high enough to ensure that noise on the deconvoluted decays is less than the maximum of the curves.

B. Fitting of a convoluted exponential

We implemented a second method of deconvolution. It consists in fitting a bi-exponential decay convoluted by the instrument response function on the experimental decay. From the parameters of the fitted bi-exponential, the derivative at the origin is computed. If the bi-exponential is written:

$$E(t) = a_1 e^{b_1 t} + a_2 e^{b_2 t}$$

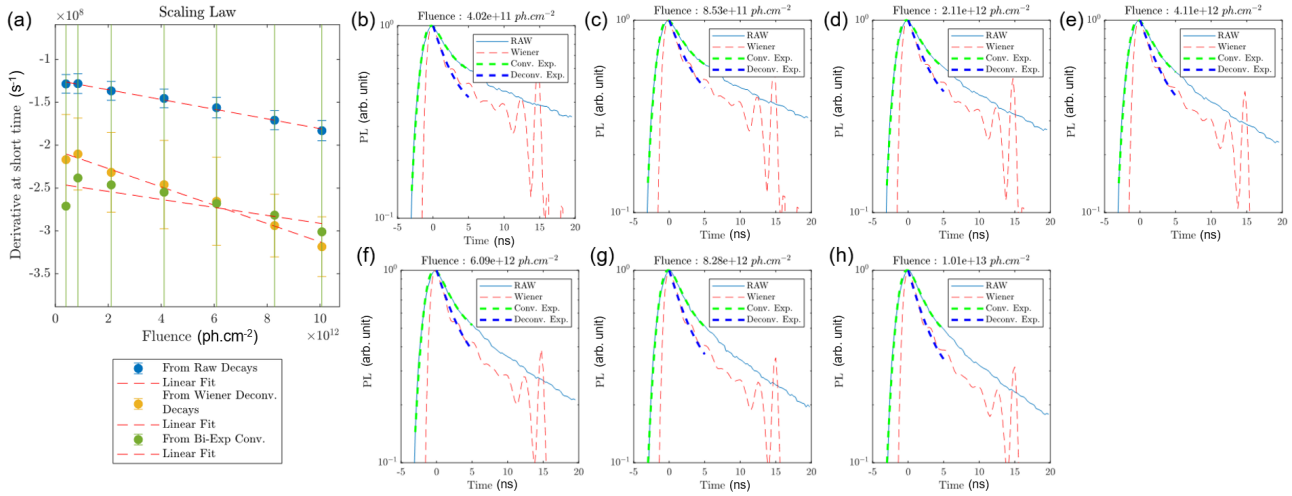

FIG. 8. Comparison of the deconvolution methods. (a) Scaling law for the three ways to compute the initial slope: from the raw decays (blue), from the Wiener deconvoluted decays (yellow) and from the parameters fitted from a bi-exponential convoluted with the instrument response function (green). (b-h) Decays and the deconvolution results. The original decay (blue line) is super-imposed with the Wiener deconvolution results (dashed red). The fitting result of a convoluted bi-exponential is presented in (dashed green), while the resulting "raw" bi-exponential is in (dashed blue).

Then the derivative at short time is computed as $a_1 b_1 + a_2 b_2$. Only three parameters are fitted as we have the normalization condition $a_1 + a_2 = 1$.

The results are shown in Figure 8. The Wiener deconvolution is also added for comparison. The fitted convoluted exponential are quite close to the experimental observations. We note that the deconvoluted bi-exponential is very close to the Wiener deconvolution result. The corresponding scaling is observed in (a). While the order of magnitude is similar for the Wiener and bi-exp method, the bi-exp method is subject to higher uncertainty. The uncertainty comes from the fitting algorithm and as the derivative is computed with three fitting parameters, all coming with an uncertainty, the total uncertainty is high, of the order of 100%. This makes us conclude that the Wiener Filter is a better method to use.

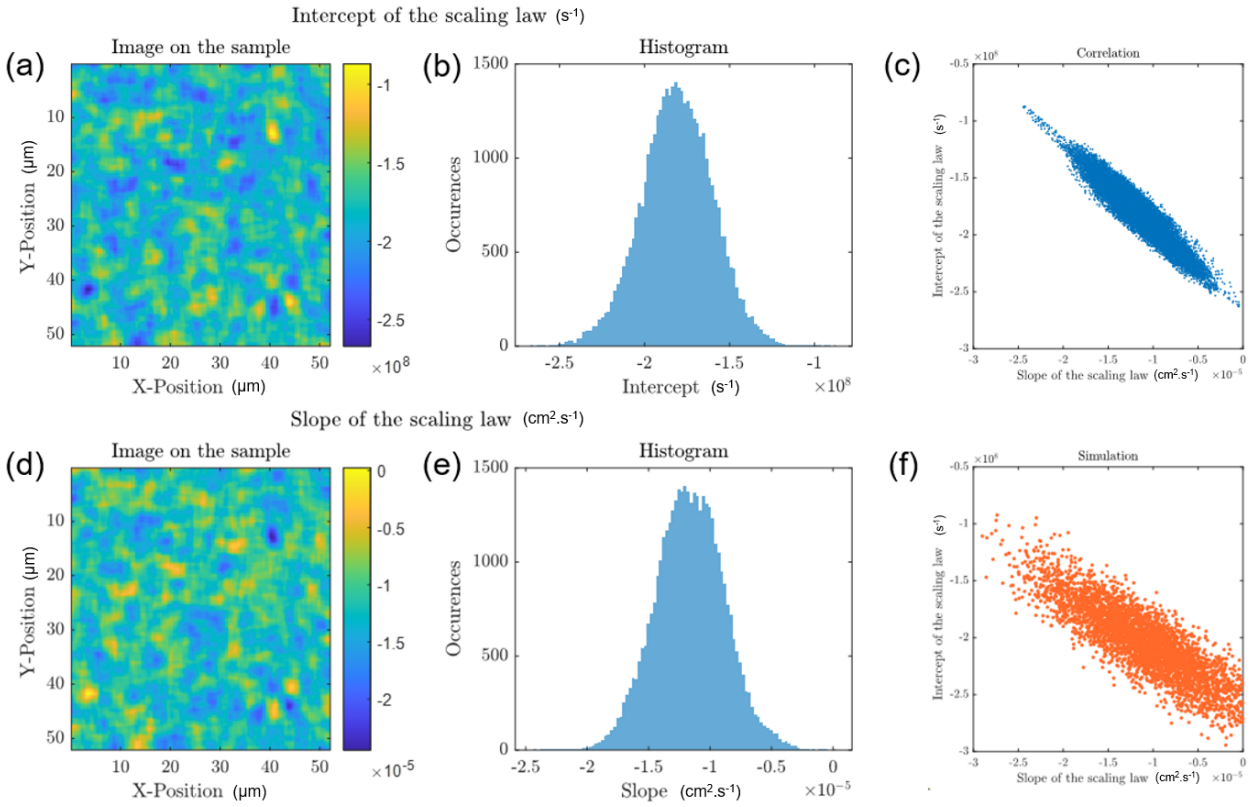

FIG. 9. Local determination of parameters. (a-b). Map and histogram of the fitted intercept for the local scalings. (d-e). Map and histogram of the fitted slope for the local scalings. (c) Experimental correlation between the two obtained parameters. The 7 fluences acquisitions were used at a local scale. A binning of 10 pixels is applied, meaning that all pixels are averaged out on a square of size 10×10 pixels. For each pixel decays are obtained. The derivative of the deconvoluted decays are computed between 0.5 and 2.5ns. The derivatives are assembled to form the scaling, which is linearly fitted. (f) Simulated correlation. Simulation of fitting linear curves with each point being multiplied by a relative error of 20%. This plot shows the fitted intercept as a function of fitted slope after noise has been simulated.

IV. LOCAL DETERMINATION OF THE SCALING

A. Homogeneous perovskite sample

To use the scaling locally, local decays are computed. For all pixel (i, j), the decay is composed of the signal of all the pixels in the square $(i \pm 5, j \pm 5)$. For each decay, the deconvolution algorithm is applied. Then the derivative is computed. Thus, for each pixel a scaling of derivative as a function of fluence is established.

If local slope and intercept are fitted, the results are given in Figure 9. We can observe that the two maps Figure 9 (a,d) are greatly negatively correlated as highlighted by Figure 9 (c). Our tests of simulated noise conclude that such correlation could appear as a simple result of measurement noise on the derivative, see (f). To perform this test we simulated 2000 scalings from an original perfectly linear scaling with values of intercept and slope equal to the values we found experimentally. From this perfectly linear scaling composed of ten points, we generated Gaussian noise centered on 1 and of standard deviation 0.2. For each of the ten points, a random variable is drawn and multiplied to the original point. Then we apply a linear fit and obtain a slope and intercept. We do this 2000 times and plot the correlation between the intercept and slope in 9 (f). We can observe a linear negative correlation between the two as observed on our experimental data.

We conclude that the independent measurement of the local slope and intercept requires more precise measurements.

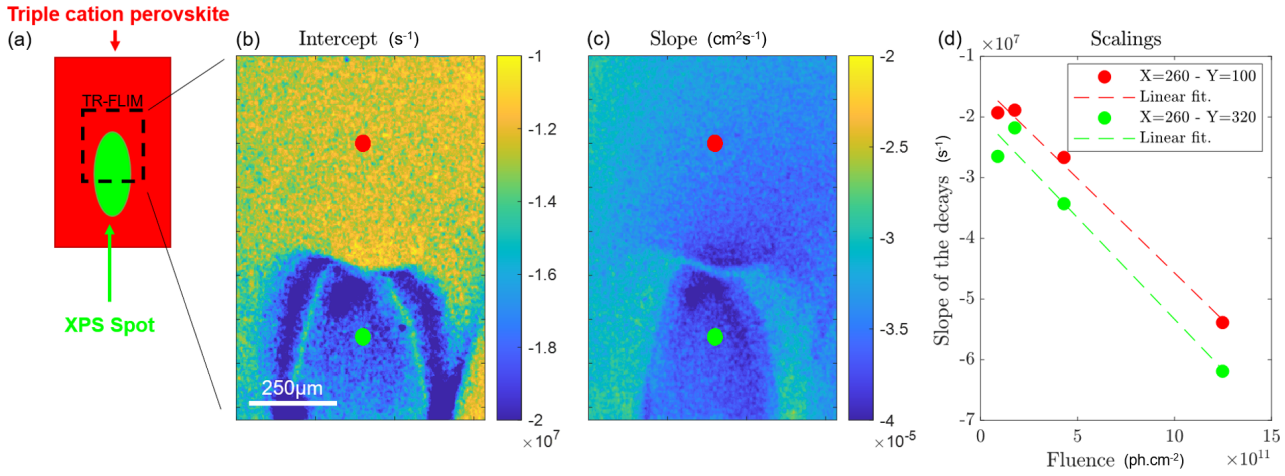

FIG. 10. (a) Scheme of the perovskite sample on glass analyzed via XPS. (b) Map of the intercept of the scaling law. (c) Map of the slope of the scaling law. (d) Two local scaling corresponding to the points in red and green in (b) and (c). We observe that while the slope of the scaling is similar inside and outside of the region exposed to X-Rays, the intercept of the scaling has changed. This means that the X-Rays did not modify the radiative recombination parameters k_2 and α, but did induce more non radiative recombination.

B. In-Homogeneous perovskite sample

To further verify that our technique allows for the interpretation of imaging data, we report here an analysis carried out on a triple cation perovskite thin film after being exposed to an X-ray beam. We acquired time resolved maps and then we applied the scaling law. In Figure 10(a) and 10(c) we show the maps of the intercept and of the slope, respectively. In both cases, the XPS spot is clearly visible, proving that the transport properties of the material have been modified by the X-rays. We then consider two points: the first on the "as deposited" sample (red) and the second within the XPS spot (green) and we draw the corresponding scaling (Figure 10(d)). On one side, we can notice that the slope of the scaling is similar in the two cases, indicating that the radiative recombination parameters, namely k_2 and α, did not evolve due to the X-rays. On the other side, the intercept values varied from -1e-7 s^{-1} to -2e-7 $^{-1}$, demonstrating an increase of the non-radiative recombination processes after beam exposure.

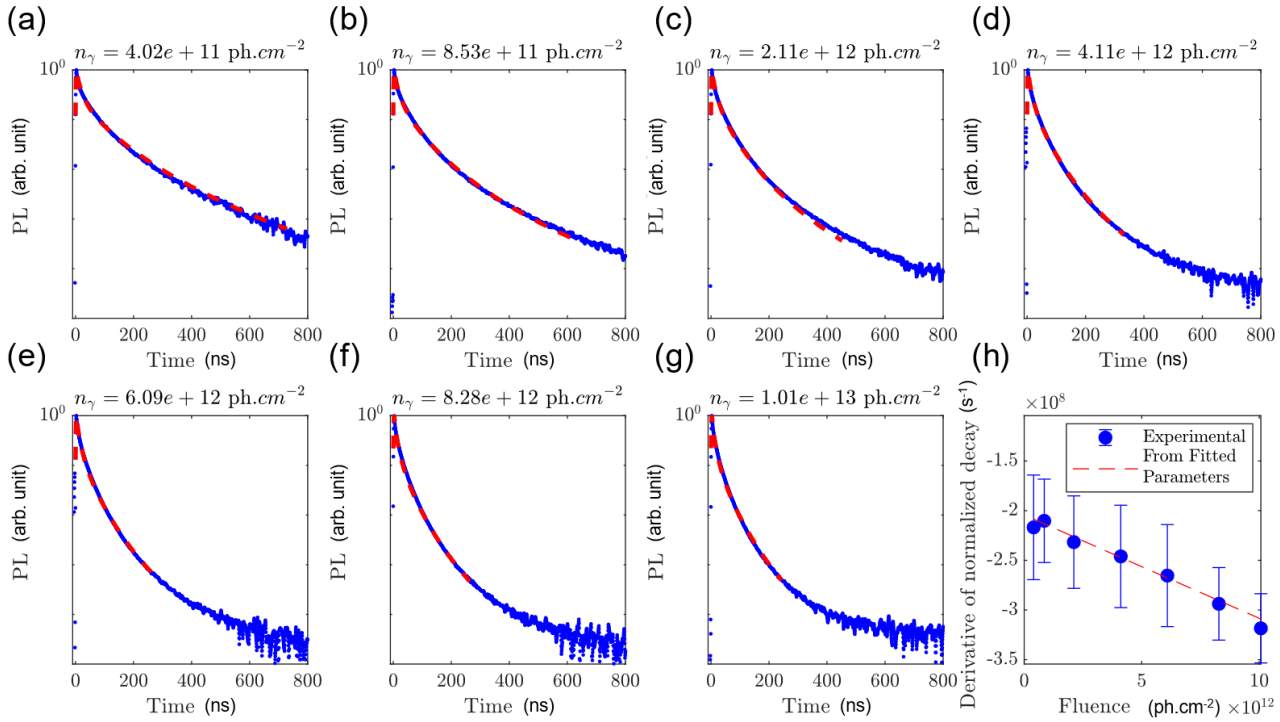

FIG. 11. Fitting the long decays with of Triple-Cation Perovskite with the Drift Diffusion Model, Strategy 2. (a-g) Fitting result (red dotted line) compared to experimental data (blue points). The experimental curves are a composition of the super-resolved decays and regular decays. The model is fitted until a level of 5×10^{-4} is reached by the experimental curves, which corresponds to the last tolerable SNR. The extracted parameters are given in Table I. (h) Scaling of the short-time derivative: from the model fitted parameters included in the theoretical formula of the scaling (red dotted line) vs. measured on the experimental deconvoluted curves (blue points). The interval for the determination of the derivative was set to be from 0.5 to 2.5ns after the maximum of the decay is reached. Error bars come from linear fitting of the log decay, which is the method used for derivative estimation.

TABLE I. Model Parameters, Strategy 2. These model parameters correspond to usual parameters for perovskite absorbers, along with fitted parameters

Symbol	Name	Value	Uncertainty	Unit
α	Absorpion coefficient	6.5×10^4	n.a.	cm^{-1}
L	Thickness	500	n.a.	nm
k_2	Radiative Recombination Coefficient	1.2×10^{-10}	n.a.	$cm^3 s^{-1}$
S_{bot}	Bottom Surface recombination velocity	0	n.a.	$cm.s^{-1}$
D	Diffusion Coefficient	3.54×10^{-3}	6%	$cm^2 s^{-1}$
k_1	Order 1 Recombination Coefficient	9.23×10^6	2%	s^{-1}
N_{bulk}	Trap-Related Density for bulk defects	4.9×10^{15}	5%	cm^{-3}
S_{top}	Top Surface recombination velocity	600	8%	$cm.s^{-1}$
N_{top}	Trap-Related Density for surface defects	1.7×10^{14}	25%	cm^{-3}

V. DRIFT DIFFUSION FIT

A. Fitting Method

The solver is coded with Matlab and uses the `pdepe` function. The equation solves for $\Delta n(z,t)$, then computes $I_{PL}(t)$ as the trapeze-computed integral of $(\Delta n(z,t))^2$. Time convolution is also conducted with trapeze-computed integral with the formula:

$$I_{PL}^{conv}(t) = \int_{-\infty}^{+\infty} dt' I_{PL}(t') h(t-t')$$

TABLE II. Correlations between fitted model Parameters, Strategy 2.

	D	S_{top}	N_{top}	k_1	N_{bulk}
D	1.00	0.10	0.78	-0.25	0.78
S_{top}	0.10	1.00	0.45	-0.57	0.29
N_{top}	0.78	0.45	1.00	-0.64	0.44
k_1	-0.25	-0.57	-0.64	1.00	0.12
N_{bulk}	0.78	0.29	0.44	0.12	1.00

with h defined in Equation 29. The fitting is realized using `lsqcurvefit` method.

The curves were fitted simultaneously on various time-spans that corresponded for each curve to the time where $I_{PL}^{norm} > 5 \times 10^{-4}$. We chose to set the bottom surface recombination velocity S_{bot} to 0, because recombination at the interface between glass and perovksite was proven to be negligible, and because our tests to include it in the fit were inconclusive.

We were able to reproduce the behavior of our experimental data with only one parameter set for all fluences, see Figure 11. The correspondence is excellent with all the curves. Not only does our model reproduce the behavior of our sample over 2 orders of magnitude of excitation, but it also reproduces quite closely the scaling of the short-time derivative as a function of fluence, as shown in Figure 11 (h). This means that the model we fitted both represents the short-time and the longer-time dynamics of our sample.

B. Uncertainties from the fit

Uncertainties are estimated using the `nlparci` method of Matlab for non-linear fitting techniques.

C. Discussion on the obtained parameters

We found $k_1 = (9.23 \pm 0.19) \times 10^6\ s^{-1}$, which could be interpreted as a lifetime $\tau = 1/k_1 = (108 \pm 3)\ ns$. This is compatible with values found in the literature in terms of orders of magnitude and precedent values obtained by our group [24].Less expected and less commonly used as a parameter in the literature is the trap-related density for bulk defects $N_{bulk} = (4.9 \pm 0.3) \times 10^{15}\ cm^{-3}$. This density can be related to the difference in energy between the trap energy and the closest band but also to the effective density of states of the corresponding band. If we assume that the defects are close to the conduction band, then $N_{bulk} = \frac{N_c}{2} \exp\left(\frac{E_t - E_c}{kT}\right)$. Our model cannot be used to determine which band the defect is closest to, nor can it disentangle if N_c or E_t is responsible for the value of N_{bulk}. What our model can prove is that this density is not negligible compared to photo-generated carrier density for our sample at long time after the pulse, even if the uncertainty for this value is quite large. The top surface recombination velocity was found to be $S_{top} = (6.0 \pm 0.5) \times 10^2\ cm.s^{-1}$. This value is in the high range of what was already found for such materials. The top surface defect related density $N_{top} = (1.7 \pm 0.4) \times 10^{14}\ cm^{-3}$ was found to be much smaller than N_{bulk}. This could indicate that the nature of the defects at the top interface is different than the bulk defects. Note that the ratio of the two densities gives access to their energy difference, which we estimate with

$$E_t^{bulk} - E_t^{top} = kT \ln\left(\frac{N_{bulk}}{N_{top}}\right) \tag{31}$$

This results in $E_t^{bulk} - E_t^{top} \approx 85\ meV$. The diffusion coeffcient we obtain is equal to $D = (3.54 \pm 0.21) \times 10^{-3}\ cm^2 s^{-1}$. This corresponds to a mobility of approximately $0.14\ cm^2 V^{-1} s^{-1}$.

D. Two fitting strategies

Strategy 1 corresponds to fitting D, k_1, N_{bulk}, S_t, N_{top} and k_2 with a starting point corresponding to the result of Strategy 2. Strategy 2 corresponds to fitting D, k_1, N_{bulk}, S_t, N_{top} with a fixed value for k_2 equal to the one obtained thanks to the scaling. A comparison of the results is given in Table III. Strategy 1 has higher uncertainties than Strategy 2, even if it has slightly smaller residuals.

TABLE III. Fitted Parameters.Comparison between Strategy 1 (k_2 fitted) and Strategy 2 (k_2 fixed to the value from the scaling). Residuals for Strategy 1 were 57.01 a.u. and for Strategy 2, 57.66. For Strategy 2 the value of k_2 was fixed to $1.2 \times 10^{-10}\ cm^3 s^{-1}$.

Symbol	Name	Strategy	Value	Uncertainty	Unit
D	Diffusion Coefficient	1	$(3.49 \pm 0.30) \times 10^{-3}$	9%	$cm^2 s^{-1}$
D	Diffusion Coefficient	2	$(3.54 \pm 0.21) \times 10^{-3}$	6%	$cm^2 s^{-1}$
k_1	Order 1 Recombination Coefficient	1	$(9.20 \pm 0.30) \times 10^{6}$	3.3%	s^{-1}
k_1	Order 1 Recombination Coefficient	2	$(9.23 \pm 0.19) \times 10^{6}$	2%	s^{-1}
N_{bulk}	Trap-Related Density for bulk defects	1	$(4.9 \pm 0.4) \times 10^{15}$	9%	cm^{-3}
N_{bulk}	Trap-Related Density for bulk defects	2	$(4.9 \pm 0.3) \times 10^{15}$	5%	cm^{-3}
S_{top}	Top Surface recombination velocity	1	640 ± 62	10%	$cm.s^{-1}$
S_{top}	Top Surface recombination velocity	2	600 ± 50	8%	$cm.s^{-1}$
N_{top}	Trap-Related Density for surface defects	1	$(1.7 \pm 0.7) \times 10^{14}$	42%	cm^{-3}
N_{top}	Trap-Related Density for surface defects	2	$(1.7 \pm 0.4) \times 10^{14}$	25%	cm^{-3}
k_2	Order 2 Recombination Coefficient	1	$(1.16 \pm 0.07) \times 10^{-10}$	5.6%	$cm^3 s^{-1}$

Bibliography.

[3] H. Jin, E. Debroye, M. Keshavarz, I. G. Scheblykin, M. B. J. Roeffaers, J. Hofkens, and J. A. Steele, It's a trap! On thenature of localised states and charge trapping in lead halide perovskites, Materials Horizons7, 397 (2020)

[21] M. Maiberg and R. Scheer, Theoretical study of time-resolved luminescence in semiconductors. II. Pulsed excitation,Journal of Applied Physics116, 123711 (2014)

[24] A. Bercegol, F. J. Ramos, A. Rebai, T. Guillemot, D. Ory, J. Rousset, and L. Lombez, Slow Diffusion and Long Lifetimein Metal Halide Perovskites for Photovoltaics, The Journal of Physical Chemistry C122, 24570 (2018)

[31] P. W¨urfel,Physics of Solar Cells(Wiley, 2005).

[38] M. Ansari-Rad and J. Bisquert, Insight into Photon Recycling in Perovskite Semiconductors from the Concept of PhotonDiffusion, Physical Review Applied10, 034062 (2018).